Available online at www.sciencedirect.com

ScienceDirect

journal homepage: www.elsevier.com/locate/he

Novel Janus 2D structures of XMoY (X, Y = O, S, Se, Te) composition for solar hydrogen production

E.V. Sukhanova [a,*], N. Sagatov [b], A.S. Oreshonkov [a,c,d], P.N. Gavryushkin [a,b,e], Z.I. Popov [a,**]

[a] Emanuel Institute of Biochemical Physics of Russian Academy of Sciences, 119334 Moscow, Russia
[b] Sobolev Institute of Geology and Mineralogy, Siberian Branch of Russian Academy of Sciences, prosp. acad. Koptyuga 3, 630090 Novosibirsk, Russia
[c] Laboratory of Molecular Spectroscopy, Kirensky Institute of Physics, Federal Research Center KSC SB RAS, 660036 Krasnoyarsk, Russia
[d] School of Engineering and Construction, Siberian Federal University, 660041 Krasnoyarsk, Russia
[e] Novosibirsk State University, Pirogova 2, 630090 Novosibirsk, Russia

HIGHLIGHTS

- 1A′-SMoTe Janus structure for photocatalytic water splitting.
- 1A′-SMoTe outstanding values of solar-to-hydrogen conversion efficiencies.
- Dynamic stability of 1A′-SMoO, SeMoS, SMoSe, SMoTe and SeMoTe.
- Calculated Raman spectra for Mo-based 1A′ Janus TMDs.

GRAPHICAL ABSTRACT

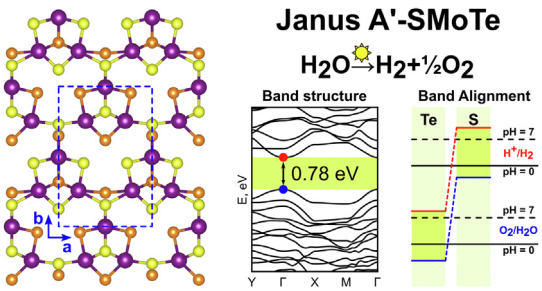

ARTICLE INFO

Article history:
Received 14 September 2022
Received in revised form
17 December 2022
Accepted 24 December 2022
Available online xxx

Keywords:
Photocatalytic water splitting
Novel materials

ABSTRACT

The successful fabrication of H-phase Janus transition metal dichalcogenides (TMDs) has received considerable interest due to its great potential in photocatalytic applications. Here, new A′-XMoY (X/Y = O, S, Se, Te) Janus-type structures belonging to the family of TMDs were theoretically investigated for the first time in terms of photocatalytic water splitting via DFT calculations. For all compounds, the Raman spectra were calculated. The SMoO, SeMoO, SMoSe, SMoTe and SeMoTe compounds are dynamically stable and are semiconductors. Among all considered structures SMoTe is the most promising candidate for solar hydrogen production because valence and conduction bands perfectly engulf the redox potentials of water at both neutral and acidic media, opposite to SMoSe, SMoO, SeMoO suitable only in the acidic media, and SeMoTe – in the neutral media. Moreover, A′-

* Corresponding author.
** Corresponding author.
E-mail addresses: yekaterina.sukhanova@phystech.edu (E.V. Sukhanova), zipcool@bk.ru (Z.I. Popov).
https://doi.org/10.1016/j.ijhydene.2022.12.286

Transition metal dichalcogenides
H_2 generation

SMoTe demonstrates the outstanding values of the solar-to-hydrogen (STH) conversion efficiencies of 54.0 and 67.1 for neutral and acidic media.

Introduction

The new ways to produce clean energy and environmentally friendly fuels belong to the idea of utilization of the widely available energy of the Sun since all energy-dependent processes on our planet indirectly or directly use the power of solar irradiation [1]. The ongoing increase in energy consumption, another issue with the current urbanization process, has created a demand for the generation of green hydrogen [1]. There is no doubt that sunshine and water, two unadulterated, renewable natural resources, are suitable for producing green hydrogen [2]. The photocatalytic splitting of water is of interest because its usage can reduce emissions of greenhouse gas, have the potential to meet growing global energy demand, solve problems related to sustainable energy supply, and mimic natural processes of solar energy effective utilization [3,4]. The concept of water decomposition into hydrogen and oxygen under solar light radiation was first demonstrated by Fujishima and Honda using a photoelectrochemical cell based on semiconductor catalysts (in particular TiO_2 electrode) [5]. An effective photocatalyst material should satisfy some conditions among which is the ability to absorb light in the visible and infrared range of the spectrum since 90% of the solar radiation energy comes from this area, it should meet the criterion of the "Honda–Fujishima effect" [3] - have a specific relationship between the conduction band minimum (valence band minimum) and the reduction potential (oxidation potential), and have an effective separation of photogenerated electrons and holes [4,6]. Despite all the benefits pristine TiO_2 shows low efficiency [5] namely due to a wide band gap (3.0–3.2 eV [7]), but its characteristics can be improved by such methods as doping or preparation of composites or heterojunctions [8–12]. Except for TiO_2-based materials, different nanoclusters [13], metal-organic frameworks [14], nanotubes [15], and nanocomposites [16–18] were considered in terms of photocatalytic water splitting reactions but the search for new technological materials for electrodes is still the primary task.

Two-dimensional nanomaterials have a high potential to be used in photocatalytic water splitting reactions [19–22] because of a large surface area leading to short migration path lengths of photogenerated carriers and due to electronic properties tunable by stain or changing the thickness. Transition metal dichalcogenides (TMDs) have already shown great potential to be used in water splitting with exceptional stability and diversity of structures and chemical compositions [23], however, TMDs are characterized by low carrier mobility which hinders the efficiency of the catalytic process [24], and only a few of them have suitable band gap value more than 1.23 eV (according to the Nernst equation) and less than 3.0 eV to efficiently utilize the solar energy [25].

The Janus monolayers having different sorts of atoms on the opposite atomic planes seem especially prospective for photocatalytic water splitting [26–28] due to the breaking of the out-of-plane structural symmetry [29] leading to the appearance of intrinsic dipole moment in the transverse direction which can improve the separation of photogenerated carriers [30,31] and help to relieve the restriction on the band gap values due to a different value of electron work function at opposite sides of the structures [32]. A lot of different Janus structures are known today [33,34], among them monolayers based on TMDs are of particular interest [28,34–37] and were successfully fabricated [38,39]. The current theoretical results demonstrate a wide range of possible structures besides H phase in the TMDs family, for example, the square MXY monolayers [40] as well as Janus T′ phases [41,42]. Besides bandgap engineering which can be realized by applying in-plane strain the properties of Janus heterostructures can be tuned by the fabrication of different heterostructures based on Janus TMDs [43–45]. Production of the Janus TMDs with a novel crystal structure offers one more degree of freedom to explore and extend their potential applications. Previously performed crystal structure prediction of possible XMoY monolayers revealed a broad variety of materials [46], among which the proposed A′-SMoSe structure seems the most promising ones due to dynamical stability and low formation energy. However, the properties of this structure in terms of photocatalytic applications have not been studied and remained unclear. In this work, the novel 2D Mo-based A′-phase of Janus TMD was examined as potential photocatalyst material for water splitting reaction by comprehensive theoretical investigation including stability, electronic properties, and optical characteristics.

Methods

Quantum chemical calculations were carried out within the density functional theory (DFT) [47,48] implemented in the VASP program package [49–51]. The exchange-correlation functional was calculated via generalized gradient approximation (GGA) in Perdew-Burke-Ernzerhof (PBE) parameterization [52]. The projector-augmented wave (PAW) [53] basis set technique was used. The energy cutoff of plane waves was set to be equal to 520 eV. The first Brillouin zone was sampled according to the Monkhorst-Pack scheme [54], and the k-point mesh of $5 \times 3 \times 1$ was chosen for structure optimization and electronic properties investigation. A vacuum region of at least 15 Å was chosen to avoid an artificial interaction between structures in a non-periodic direction. To obtain a deeper knowledge of the electronic properties of Janus XMoY (X/Y = O, S, Se, Te) structures we employed screened hybrid

Please cite this article as: Sukhanova EV et al., Novel Janus 2D structures of XMoY (X, Y = O, S, Se, Te) composition for solar hydrogen production, International Journal of Hydrogen Energy, https://doi.org/10.1016/j.ijhydene.2022.12.286

functional of Heyd-Scuseria-Ernzerhof (HSE06) [55] to estimate the bandgaps more accurately as the GGA-PBE functional generally underestimates the bandgap [55]. For atomic structure visualization, we used VESTA [56] software. The phonon calculations were carried out using the PHONOPY program package [57]. Charge redistribution in all considered systems was studied by the Bader charge analysis [58,59]. The climbing image nudged elastic band (CI-NEB) method [60,61] was used to calculate the barrier values for the phase transition.

The Cambridge Serial Total Energy Package (CASTEP code) [62] based on density functional theory is employed to simulate Raman spectra [63] of investigated A' Janus structures. The local density approximation was used and the plane wave cutoff energy for norm-conserving pseudopotentials was set to 400 eV for SeMoTe, 650 eV for SMoTe and SMoSe, and 750 eV for SeMoO and SMoO. The Brillouin zone was sampled using the Monkhorst-Pack scheme with k-point sampling no more than 0.05 2π/Å. All considered structures were optimized with the next convergence criteria: maximum forces should be less than 0.03 eV/Å, and maximum stress is no more than 0.05 GPa. The Raman spectra for all compounds were simulated by a 10 cm^{-1} Lorentzian broadening. A similar scheme was successfully used before for the reproduction of the H-SMoSe structure Raman spectrum [64].

Results and discussions

The atomic structure of the considered A′ phase was earlier proposed in Ref. [46]. There are 6 molybdenum atoms, 6 atoms of X-type, and 6 atoms of Y-type in the unit cell of Janus A′ phase (see Fig. 1a). The corresponding unit cell parameters of the examined monolayers are presented in Table S1. Considered A′ phase is characterized by the triclinic symmetry (see Fig. 1a) and Mo atoms are arranged similarly as nodes in the Kagome lattice. The Mo-X and Mo-Y bond lengths (see Table S2) correlate well with ionic radii increasing in the row from O to Te.

To estimate the thermodynamic stability of considered monolayers we compared the energies of A′ Janus structures with the energies of other TMDs Janus structures in well-known H, T, and T′ phases with the same chemical composition as $\Delta E = E_{XMoY} - E_{H-XMoY}$, where E_{XMoY} is the energy of considered phase of XMoY Janus structure, E_{H-XMoY} is the energy of H-XMoY Janus structure (see Fig. 1b and Table S3). The obtained values of ΔE for well-known Janus phases correlates well with previously reported results [36,42,65]. Janus structure of the H phase was found to be the most energetically favorable for most considered chemical compositions except for OMoTe for which T′ phase is the most energetically favorable. Our calculations showed that the energy of the 1A′ Janus phase is close to the energy of the T-phase with the same chemical composition, and the energy difference is less than 0.2 eV/f.u [42].

The dynamic stability of the A′ Janus structures was investigated through the calculations of phonon dispersion spectra. Based on obtained results only the OMoTe structure does not demonstrate dynamic stability due to the essential contribution in the imaginary part of phonon spectra (Fig. S1). Other considered structures have small bulges in the vicinity of the Γ-point (Fig. S1) which can be attributed to the lack of rotational invariance consideration [66,67], for example, because of using insufficient size supercell in phonon calculation. Therefore, we carried out additional calculations within the Hiphive program [68] which proved the dynamic stability of all considered structures except for OMoTe monolayer (see Fig. S2).

We also studied the mechanical properties of Janus XMoY (X/Y = S, Se, Te, O) TMDs by considering the elastic modulus

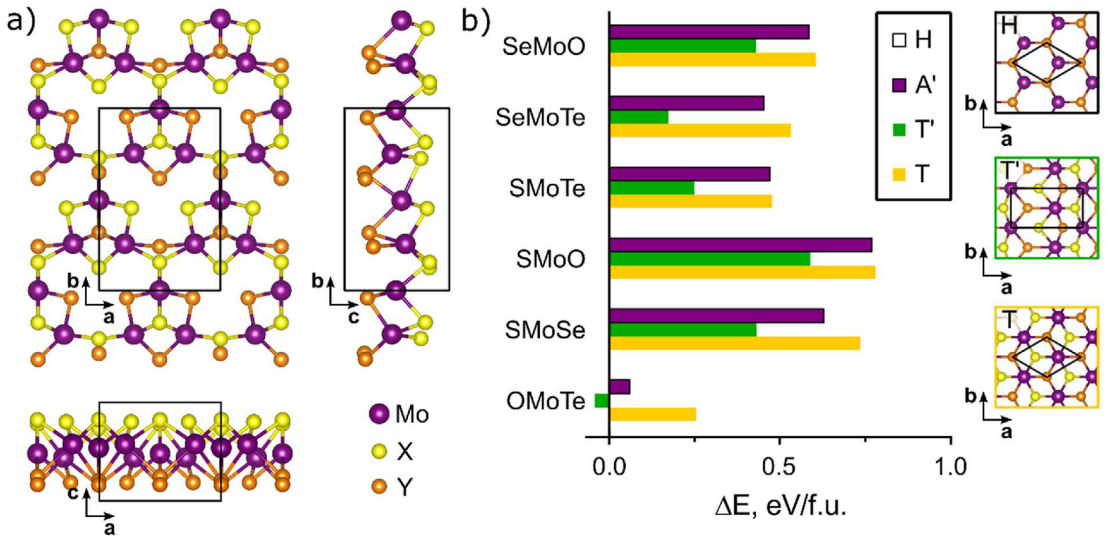

Fig. 1 – (a) The top and side views of the atomic structure of the A′ phase of Janus XMoY (X/Y = S, Se, Te, O). By purple, yellow/orange colors molybdenum and different chalcogen (S, Se, Te, O) atoms are depicted. The unit cell is highlighted by a black solid line. (b) The energy difference between the A′ (violet), T′ (green), and T (orange) phases and the H phase of TMD Janus XMoY per formal unit (eV/f.u.). (For interpretation of the references to colour in this figure legend, the reader is referred to the Web version of this article.)

Please cite this article as: Sukhanova EV et al., Novel Janus 2D structures of XMoY (X, Y = O, S, Se, Te) composition for solar hydrogen production, International Journal of Hydrogen Energy, https://doi.org/10.1016/j.ijhydene.2022.12.286

constants using the stress-strain relations (see Supporting information section SIII). The values obtained (see Table S4) allow us to additionally estimate the stability of Janus structures within Born elastic criteria: $C_{11} > 0$, $C_{11}C_{22} > C_{12}^2$, $C_{66} > 0$ [69,70]. We found that all considered Janus structures except for OMoTe satisfy the elastic stability condition. Therefore, based on phonon spectra analysis and elastic criteria we do not further consider the A′-OMoTe Janus structure. Using obtained values of C_{ij} constants we calculated the values of 2D Young's moduli in the Cartesian [10] and [010] directions which is the measure of in-plane stiffness, and the corresponding Poisson's ratios describing the mechanical response of the structure to the applied external load [71]. The angular-dependent results for Young's moduli and Poisson's ratios are shown in Fig. S3. Obtained results showed that A′-SMoSe, A′-SeMoTe, and A′-SMoTe structures have significantly anisotropic atomic structure, while A′-SeMoO and A′-SMoO monolayers display very small anisotropy. The 2D linear elastic constants calculated for A′-Janus structures are lower than those of the H and T′ phases with the same chemical composition due to the less dense structure of A′ Janus TMD leading to a much softer nature compared with other Janus phases (see Table S4) which is good for flexible electronics due simplicity to achieve in-plane strains of high magnitude. The largest value of 2D Young's moduli corresponds to the A′-SMoO structure (74.28 and 43.38 Nm^{-1} for the Cartesian [10] and [010] directions, respectively) which is nearly two and four times less than the value for the H-SMoO [72,73]. We can also notice that the exchange of one surface of the A′ phase by S or Se atoms leads to the Mo-Mo bonds strengthening and thus the in-plane stiffness is enhanced compared with surfaces formed by O or Te atoms. Regarding the Poisson's ratio, we find that in the case of the Cartesian [10] direction the values for all considered A′ Janus XMoY are significantly larger than 0.5 meaning that they are very soft in the [10] direction due to the porous structure which additionally indicates the anisotropic nature of the phase. Such significantly large Poisson's ratios suggest a sensitive structural response to the applied external stress, which can be useful for band gap engineering or, for example, piezoelectricity.

To assess the possibility of A′ Janus structures fabrication we considered some of the possible phase transition pathways from the known H and T Janus phases by examining the SMoSe chemical composition as an example (see Supporting information section SIV). We estimated the energies of phase transitions from H- and T-SMoSe structures to A′-SMoSe and the values are 1.589 eV and 0.674 eV per formula unit, respectively. We found that the transition from the H-phase to the A phase is endothermic, while from the T phase to A′ is exothermic. The barrier value for the transition from H to A′-SMoSe phases is comparable to the value for the transition from the H to the T phase of MoS_2 (1.5 eV [74,75]). At the same time, the energy for the reverse transition (from T to H phase) is 0.68 eV [76], which is also comparable to the transition barrier from the T to A′ phase. It should be noted that the phase transition barrier in 2D TMDs can be lowered by doping with electrons by charge transfer [74,75]. Moreover, it was shown that the transition from the T to the H phase can be induced during in situ scanning transmission electron microscopy experiments [77]. The above facts provide prerequisites for the experimental production of the new A′ Janus phases.

Raman spectroscopy method is a powerful tool for the investigation and identification of different nanomaterials including 2D ones [78]. The interpretation and analysis of experimental Raman spectra can be significantly simplified by comparison with the theoretically calculated spectra within quantum-chemical methods. Therefore, to facilitate of the process of experimental identification and search of novel A′ Janus structures we additionally studied theoretically predicted Raman spectra for dynamically stable A′ Janus structures. Previously proposed computational model and parameters showed an excellent agreement with known experimental data for H-MoSSe structure (see Ref. [64]), therefore in this paper we applied the model to investigate the features of A′ Janus structures Raman spectra (see Fig. 2). The conventional cell of the A' phase has 18 atoms (similar to the H' phase considered in Ref. [64]) and is described within the C1 crystallographic space group, thus it has 54 vibrational modes represented by A. Three of these modes are related to acoustical vibrations while the remaining modes should be Raman active. The position and intensity of spectral bands depend on chemical composition. For the convenience of presentation, the spectral profiles shown in Fig. 2 were similarly rated according to the most intense peak in each spectrum. Spectral ranges for A′-SeMoTe, A′-SMoTe, A′-SMoSe, A′-SeMoO and A′-SMoO may be listed as 44–333 and 47–443 cm^{-1} (Fig. 2a), 51–457 cm^{-1} (Fig. 2b), 35–749 and 49–763 cm^{-1} (Fig. 2c), respectively. A side-by-side comparison of all spectra up to 800 cm^{-1} is presented in Fig. 2d.

The low-wavenumber part of the A′-SeMoTe Raman spectrum (below 100 cm^{-1}) is related to vibrations of Se/Mo/Te atomic groups and corresponding spectral lines have low intensity (Fig. 2a). The weak bands at 107 and 128 cm^{-1} are associated with Te and Se in-plane translation, respectively. The Mo-Te stretching-like vibrations with a small contribution of Se movements appeared via strong lines at 181, 211, and 272 cm^{-1}. The remaining three strong bands at 289, 313 and 333 cm^{-1} are Mo-Se stretching, see Fig. 2. The A′-SMoTe spectrum up to 225 cm^{-1} (Fig. 2a) is similar to A′-SeMoTe. The weak band at 122 cm^{-1} related to S (with a small contribution of Mo ions) translation. A group of strong bands from 180 to 258 cm^{-1} is Mo-Te stretching mixed with S translations. The strong lines from 288 to 416 cm^{-1} are Mo-S vibrations. A single strong peak at 442 cm^{-1} can be described as sulfur out-of-plane vibration.

The most complex spectral profile is obtained for the A' phase of SMoSe. Nevertheless, individual high-intensity spectral bands are observed in the spectrum. The Mo-S stretching-like vibrations are located from 345 to 391 cm^{-1} (Fig. 2b). The strong wide band between 442 and 456 cm^{-1} is an out-of-plane vibration of sulfur ions. The several combinations of in-plane and in-plane/out-of-plane S/Se vibrations appeared via remaining intensity peaks as marked in Fig. 2b. The intensity of low-wavenumber lines for the studied phase of A′-SMoSe is very low.

The simulated Raman spectrum of A′-SeMoO is dominated by oxygen vibration peaks at 490 and 655 cm^{-1}, see Fig. 2c, which are a combination of oxygen out-of-plane/in-plane and oxygen out-of-plane movements, correspondingly. The

Please cite this article as: Sukhanova EV et al., Novel Janus 2D structures of XMoY (X, Y = O, S, Se, Te) composition for solar hydrogen production, International Journal of Hydrogen Energy, https://doi.org/10.1016/j.ijhydene.2022.12.286

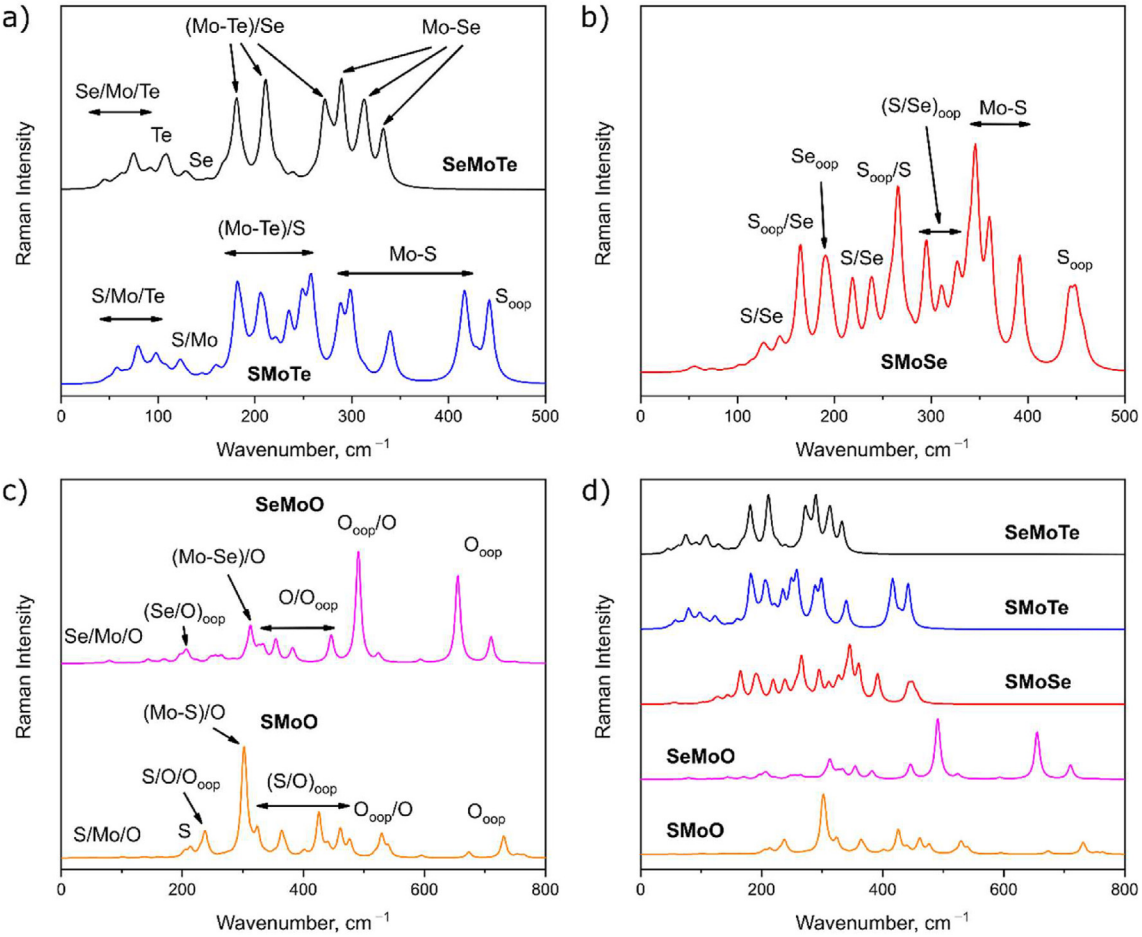

Fig. 2 – Calculated Raman spectra for A' phase for (a) SeMoTe and SMoTe, (b) SMoSe, (c) SeMoO and SMoO. A comparison of all obtained spectra is presented in (d). The "oop" subscript corresponds to the designation of out-of-plane vibrations.

medium intensity spectral bands from 325 to 445 cm^{-1} are in-plane/out-of-plane vibrations of O atoms. The medium peak at 312 cm^{-1} is a Mo-Se stretching-like vibration combined with in-plane O translations. Group of weak lines below 275 cm^{-1} related to out-of-plane Se/O vibrations. The Raman spectrum of A′-SMoO, see Fig. 2c, is dominated by the strongest line at 301 cm^{-1}, which is related to Mo-S stretching-like vibration with an admixture of O movements. As can be seen from Fig. 2c, the range of out-of-plane and out-of-plane/in-plane O vibrations is a bit shifted to the higher wavenumbers, while the middle part of spectra is a S/O out-of-plane translation. Spectral bands between 200 and 250 cm^{-1} are translations of sulfur and sulfur/oxygen ions. The spectral profile in the low-wavenumber part has very weak spectral peaks similar to A′-SeMoO.

Variation of simulated Raman spectra of A′-XMoY Janus monolayers concerning chemical composition (X/Y = S, Se, Te, O) is shown in Fig. 2d. It is seen that a decrease in the atomic weight of chalcogen atoms shifts spectral lines to the high-wavenumber region. The spectrum of each studied structure has a unique profile that is more complex in comparison with known H, T, and T′-XMoY Janus types [64]. This, in turn, makes it possible to make an unambiguous identification of the structures obtained experimentally by the Raman scattering method.

To study the electronic properties of considered structures we calculated the electronic band structures for dynamically stable A′ phases. The electronic band structures calculated via HSE06 hybrid functional are presented in Fig. 3. All considered A′-XMoY structures exhibit nonmagnetic semiconducting electronic properties: SeMoO, SMoO, and SMoSe are indirect semiconductors with band gap (E_g) of 1.15, 1.50 and 1.54 eV, respectively. The conduction band minimum (CBM) is on the ΓX-path for SeMoO and SMoSe and the XM-path for SMoO structure. The valence band maximum (VBM) lies at the X, X and Γ points for SeMoO, SMoO, and SMoSe. Janus SeMoTe, and SMoTe are direct semiconductors with a band gap of 0.84 and 0.78 eV, respectively (see Fig. 3), and with the CBM and VBM lying at the Γ point. The corresponding to CBM and VBM charge densities spatial distribution are presented in Fig. S6.

Semiconducting properties suggest the possible application of A′ Janus structures in photocatalytic water splitting reactions. To verify this ability, first, we considered optical properties, because an excellent optical absorption is a necessary condition for the application of a 2D photocatalyst because the first step of water-splitting is the appearance of electron-hole pairs due to photon absorption. For these aims we considered wavelength-dependent complex dielectric function $\varepsilon(\lambda) = \varepsilon_1(\lambda) + i\varepsilon_2(\lambda)$, in which the real part was calculated by Kramers-Kronig relation and the

Please cite this article as: Sukhanova EV et al., Novel Janus 2D structures of XMoY (X, Y = O, S, Se, Te) composition for solar hydrogen production, International Journal of Hydrogen Energy, https://doi.org/10.1016/j.ijhydene.2022.12.286

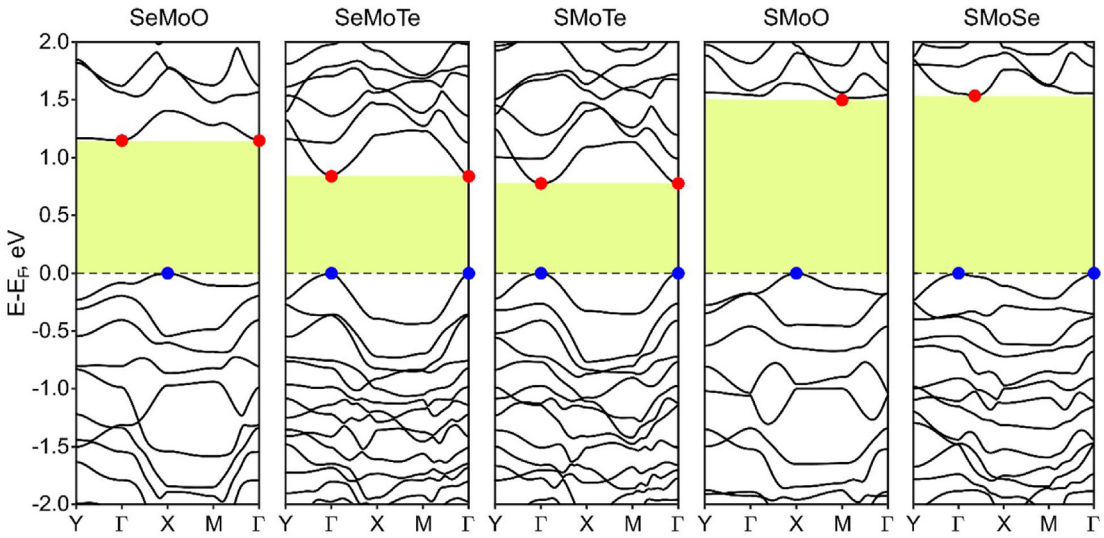

Fig. 3 – Electronic band structures for A′ Janus XMoY (X/Y = O, S, Se, Te) structures within HSE06 hybrid functional.

imaginary part was determined by the sum over empty states [79,80]. The extinction coefficient which is the measure of how strong the material absorb the incident light was found as: $K(\lambda) = \left[\frac{\sqrt{\varepsilon_1^2(\lambda)+\varepsilon_2^2(\lambda)}-\varepsilon_1(\lambda)}{2}\right]^{1/2}$, and the absorption coefficient which indicates describes the intensity attenuation of the light passing through a nanostructure was found as $\alpha(\lambda) = \frac{2\sqrt{2}\pi}{\lambda}\left[\frac{\sqrt{\varepsilon_1^2(\lambda)+\varepsilon_2^2(\lambda)}-\varepsilon_1(\lambda)}{2}\right]^{1/2}$. The calculated wavelength dependence of the extinction coefficient and the absorption coefficient in the direction parallel and perpendicular to the surface of A′ Janus monolayers are shown in Fig. 4. For comparison, we also calculated the same dependencies for the H-SMoSe monolayer (Fig. 4, grey), and the wavelength dependence of the absorption coefficient in the transverse and perpendicular to the surface directions for the H-SMoSe monolayer agrees well with the data presented in Refs. [81–83].

It should be noticed that both the extinction and absorption spectrum of A′-Janus phases exhibit strong anisotropy among two directions of polarization. Calculated spectra for different chemical compositions have generally the same forms and are different in intensities and peak positions. With the irradiation of A′ Janus structures by the light with parallel polarization, the maxima absorption peak is observed at 210–350 nm (UV region). The peak next in intensity is observed at 450–600 nm which corresponds to the visible light range. It should be noted that the maximum value of the $K_{\|}$ for A′-MoSeTe exceeds the corresponding value for H-MoSSe monolayer. The irradiation of considered A′ structures by the light with normal polarization results in the maxima at 150–220 nm (UV region) like H-MoSSe which has one more peak at 100–120 nm. The calculated wavelength dependence of the absorption coefficient in the direction parallel and perpendicular to the surface of A′ Janus monolayers is shown in Fig. 4c and d. A′-XMoY Janus structures are characterized by strong absorption intensity in a visible light region which is nearly 50% of solar light power (see Fig. 4c and d). Moreover, in the case of irradiation by the light with parallel polarization the maximum value for A′-SeMoTe (see Fig. 4c, black line) exceeds the value for H-MoSSe structure (see Fig. 4, grey line). The absorption coefficients peak in visible and ultraviolet light region are more than 10^5 cm^{-1} which indicates high efficiency of the solar energy utilization comparing to the values of other conventional optical-absorber materials like CdTe, CIGS, and hybrid halide perovskites [84,85]. Therefore, A′ Janus materials are promising to be applied in photocatalytic water splitting and optoelectronic devices.

One of the features of Janus monolayers is the existence of intrinsic vertical dipole moment. Different sorts of atoms on the opposite atomic planes result in structure polarity and the appearance of dipole moment leading to a build-in electrical field that may enhance the separation between the electrons and holes (see Fig. S7) [86,87]. The calculated values of dipole moments are presented in Table S5. The resulting values of the perpendicular to the x-y plane dipole moments correlates well with the electronegativity difference of chalcogen atoms in the Janus structure. The largest value of the dipole moment corresponds to the A′-SMoO structure (0.71 D per unit cell), while A′-SMoTe has the lowest dipole moment (0.11 D per unit cell). It should be noted that the dipole moments of A′ Janus structures are comparable with the values for H Janus phases (Table S5). The existence of intrinsic dipole moment results in an electrostatic potential difference leading to different values of work functions of each side of the Janus monolayer. The obtained values are presented in Table S6.

An important parameter characterizing the possibility of monolayer application in photocatalytic water splitting reaction is the ratio between the band edge (VBM and CBM) positions and the redox potentials of water [30] (see Fig. 5) which are pH-dependent [88]. To be suitable for photocatalyst VBM of the material must be lower than the level of O_2/H_2O to provide OER while CBM must be higher than the H^+/H_2 to ensure HER.

Please cite this article as: Sukhanova EV et al., Novel Janus 2D structures of XMoY (X, Y = O, S, Se, Te) composition for solar hydrogen production, International Journal of Hydrogen Energy, https://doi.org/10.1016/j.ijhydene.2022.12.286

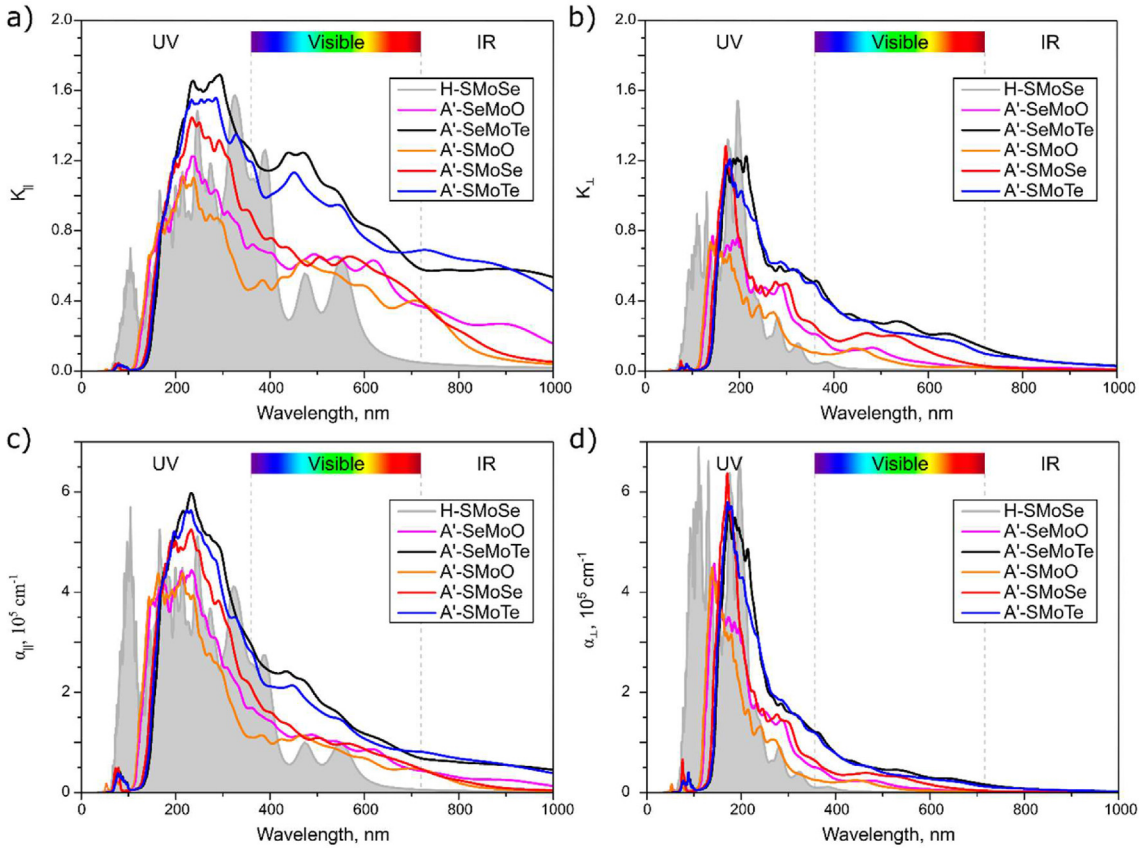

Fig. 4 – (a, b) Wavelength dependence of the extinction coefficient and (c, d) energy dependence of the absorption coefficient in the (a, d) transverse and (b, c) perpendicular to the surface directions of A′ Janus XMoY (X/Y = O, S, Se, Te) and H-SMoSe structures calculated with a HSE06 functional.

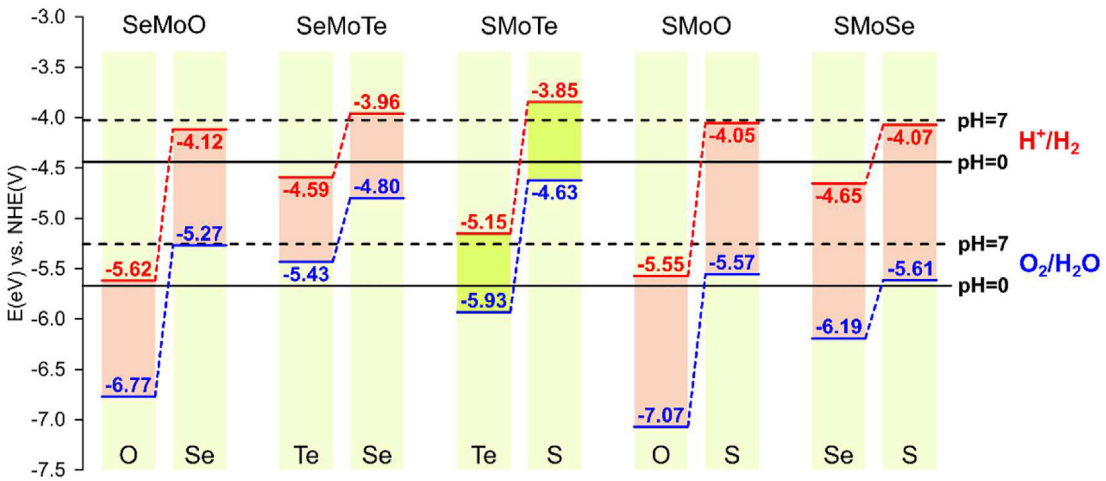

Fig. 5 – Band edge positions of 1A′ Janus XMoY (X, Y = O, S, Se, Te) structures compared with the redox potentials of water based on results obtained by HSE06 functional. The values are given concerning the vacuum level (in eV). The redox potentials of water are denoted as the violet and pink dashed lines for pH = 0 and pH = 7 [88]. (For interpretation of the references to colour in this figure legend, the reader is referred to the Web version of this article.)

As follows from Fig. 5, the A′-SeMoTe monolayer is a perfect candidate in photocatalytic applications because its band gap positions correlate with water splitting potential at both neutral and acidic (pH = 0) media. However, other considered structures are suitable not in all media: SMoSe, SMoO, and SeMoO structures are promising candidates for both HER and OER only in the case of acidic media, while SeMoTe – in the neutral media.

Please cite this article as: Sukhanova EV et al., Novel Janus 2D structures of XMoY (X, Y = O, S, Se, Te) composition for solar hydrogen production, International Journal of Hydrogen Energy, https://doi.org/10.1016/j.ijhydene.2022.12.286

Table 1 – The energy conversion efficiency of light absorption (η_{abs}), carrier utilization (η_{cu}), the influence of intrinsic electric field (η_f), the STH (η_{STH},) and the corrected STH (η'_{STH}) values for dynamically stable A' Janus XMoY (X, Y = O, S, Se, Te) structures for photocatalytic process in neutral and acid media.

η, %	Media	A′-SMoTe	A′-SMoSe	A′-OMoS	A′-OMoSe	A′-SeMoTe
η_{abs}	pH = 7	92.0	59.4	61.4	61.0	–
	pH = 0	92.0	–	–	–	89.4
η_{cu}	pH = 7	58.6	51.4	57.9	57.7	–
	pH = 0	72.9	–	–	–	45.2
η_f	pH = 7	63.5	87.4	69.5	69.9	–
	pH = 0	58.4	–	–	–	82.8
η_{STH}	pH = 7	54.0	30.6	35.6	35.2	–
	pH = 0	67.1	–	–	–	40.5
η'_{STH}	pH = 7	34.3	26.7	24.7	24.6	–
	pH = 0	39.2	–	–	–	33.5

We also studied the solar-to-hydrogen (STH) conversion efficiencies within the method proposed by Yang et al. [89], according to which assuming 100% efficiency of the catalytic reaction the STH efficiency (η_{STH}) can be estimated as the product of the efficiency of light absorption (η_{abs}) and carrier utilization (η_{cu}):

$$\eta_{STH} = \eta_{abs} \times \eta_{cu}$$

$$\eta_{abs} = \frac{\int_{E_g}^{\infty} P(h\omega)d(h\omega)}{\int_{0}^{\infty} P(h\omega)d(h\omega)}$$

$$\eta_{cu} = \frac{\Delta G_{H_2O} \int_{E}^{\infty} \frac{P(h\omega)}{h\omega} d(h\omega)}{\int_{E_g}^{\infty} P(h\omega)d(h\omega)}$$

where $P(h\omega)$ is the AM1.5G solar energy flux at the photon energy $h\omega$; ΔG_{H_2O} is the free energy of water splitting, E is the photon energy that can be utilized in the catalytic reaction defined as:

$$E = \begin{cases} E_g, \chi(H_2) \geq 0.2, \chi(O_2) \geq 0.6 \\ E_g + 0.2 - \chi(H_2), \chi(H_2) < 0.2, \chi(O_2) \geq 0.6 \\ E_g + 0.6 - \chi(O_2), \chi(H_2) \geq 0.2, \chi(O_2) < 0.6 \\ E_g + 0.8 - \chi(H_2) - \chi(O_2), \chi(H_2) < 0.2, \chi(O_2) < 0.6 \end{cases}$$

where $\chi(H_2)$, $\chi(O_2)$ are over potentials for Hydrogen and Oxygen Evolution Reactions, respectively. Considering the intrinsic electric field existing in Janus monolayers the modified STH efficiency of the photocatalytic water splitting reaction can be estimated as:

$$\eta'_{STH} = \eta_{abs} \times \eta_{cu} \times \eta_f$$

$$\eta_f = \frac{\int_{0}^{\infty} P(h\omega)d(h\omega)}{\int_{0}^{\infty} P(h\omega)d(h\omega) + \Delta\Phi \int_{E_g}^{\infty} \frac{P(h\omega)}{h\omega} d(h\omega)}$$

where $\Delta\Phi$ is the work function difference of the opposite surfaces of Janus structure. The obtained values of the STH efficiencies are presented in Table 1 while the values of $\chi(H_2)$, $\chi(O_2)$, $\Delta\Phi$ are presented in Table S7. A′-SMoTe which is the most promising structure meet the standard for commercial applications because the values of the STH and corrected STH efficiencies are more than commercialization limit of 10% [90] and, moreover, the values obtained for A′-SMoTe Janus structure exceed the corresponding values for H-SWSe monolayer [91] and other considered structures [92]. However, it should be noted that the obtained values of η_{STH} and η'_{STH} are larger than the conventional theoretical limit (18%) and are comparable with the experimentally obtained values [93].

Strain-engineering is a powerful tool to modulate the electronic properties of the nanomaterial [94,95], moreover, external strain can significantly impact the catalytic properties of the material [96,97], for example, cause the shift of the band edge positions and changing the band gap value. We examined the effect of monodirectional and bidirectional expansions and compressions on the catalytic properties of A′ Janus structures (see Supporting information section SVI: Figs. S8–S12). Performed quantum-chemical calculations showed that A′-SMoTe Janus structure preserves catalytic characteristics either in acid or neutral media even when stretched both in one and both directions (see Fig. S8) which indicate a high potential of this structure. It should be noted that A′-SMoSe Janus monolayer could be used for overall photocatalytic water splitting under, for example, compressed by 5% (see Fig. S10).

Conclusion

The comprehensive theoretical investigation of novel Mo-based Janus A′ TMDs revealed that the A′-SMoTe have outstanding values of solar-to-hydrogen (STH) conversion efficiencies of 54.0% and 67.1% for neutral and acidic media, which makes this material a perfect candidate for photocatalytic water splitting. The ratio between the band edge (VBM and CBM) positions of A′ Janus SeMoTe and the redox potentials of O_2/H_2O and H^+/H_2 make the structure suitable in both neutral and acidic media. Besides, other considered structures: SMoSe, SMoO, and SeMoO are suitable for acidic media, while SeMoTe – is for the neutral media and the values

Please cite this article as: Sukhanova EV et al., Novel Janus 2D structures of XMoY (X, Y = O, S, Se, Te) composition for solar hydrogen production, International Journal of Hydrogen Energy, https://doi.org/10.1016/j.ijhydene.2022.12.286

of STH exceed the conventional theoretical limit (18%). The predicted Raman spectra can be useful for future experimental verification of proposed structures which can be potentially fabricated from known H and T phases, for example, via strain-induced structural phase transition. We showed that the family of TMDs can still contain some new dynamically stable structures with outstanding properties for practical application.

Declaration of competing interest

The authors declare that they have no known competing financial interests or personal relationships that could have appeared to influence the work reported in this paper.

Acknowledgments

The authors acknowledge financial support from Russian Science Foundation (№ 21-73-20183). The authors are grateful to the Joint Supercomputer Center of the Russian Academy of Sciences and to the Information Technology Centre of Novosibirsk State University for providing access to the cluster computational resources.

Appendix A. Supplementary data

Supplementary data to this article can be found online at https://doi.org/10.1016/j.ijhydene.2022.12.286.

REFERENCES

[1] Dawood F, Anda M, Shafiullah GM. Hydrogen production for energy: an overview. Int J Hydrogen Energy 2020;45:3847–69. https://doi.org/10.1016/j.ijhydene.2019.12.059.
[2] Esapour K, Abbasian M, Saghafi H. Intelligent energy management in hybrid microgrids considering tidal, wind, solar and battery. Int J Electr Power Energy Syst 2021;127:106615. https://doi.org/10.1016/j.ijepes.2020.106615.
[3] Fang Y, Zheng Y, Fang T, Chen Y, Zhu Y, Liang Q, et al. Photocatalysis: an overview of recent developments and technological advancements. Sci China Chem 2020;63:149–81. https://doi.org/10.1007/s11426-019-9655-0.
[4] Gupta A, Likozar B, Jana R, Chanu WC, Singh MK. A review of hydrogen production processes by photocatalytic water splitting – from atomistic catalysis design to optimal reactor engineering. Int J Hydrogen Energy 2022;47:33282–307. https://doi.org/10.1016/j.ijhydene.2022.07.210.
[5] Fujishima A, Honda K. Electrochemical photolysis of water at a semiconductor electrode. Nature 1972;238:37–8. https://doi.org/10.1038/238037a0.
[6] Schneider J, Matsuoka M, Takeuchi M, Zhang J, Horiuchi Y, Anpo M, et al. Understanding TiO_2 photocatalysis: mechanisms and materials. Chem Rev 2014;114:9919–86. https://doi.org/10.1021/cr5001892.
[7] Ge M, Cai J, Iocozzia J, Cao C, Huang J, Zhang X, et al. A review of TiO_2 nanostructured catalysts for sustainable H_2 generation. Int J Hydrogen Energy 2017;42:8418–49. https://doi.org/10.1016/j.ijhydene.2016.12.052.
[8] Du S, Lian J, Zhang F. Visible light-responsive N-doped TiO_2 photocatalysis: synthesis, characterizations, and applications. Trans Tianjin Univ 2022;28:33–52. https://doi.org/10.1007/s12209-021-00303-w.
[9] Basavarajappa PS, Patil SB, Ganganagappa N, Reddy KR, Raghu AV, Reddy CV. Recent progress in metal-doped TiO_2, non-metal doped/codoped TiO_2 and TiO_2 nanostructured hybrids for enhanced photocatalysis. Int J Hydrogen Energy 2020;45:7764–78.
[10] Eidsvåg H, Bentouba S, Vajeeston P, Yohi S, Velauthapillai D. TiO_2 as a photocatalyst for water splitting—an experimental and theoretical review. Molecules 2021;26:1687.
[11] Ding Q, Gou L, Wei D, Xu D, Fan W, Shi W. Metal-organic framework derived Co_3O_4/TiO_2 heterostructure nanoarrays for promote photoelectrochemical water splitting. Int J Hydrogen Energy 2021;46:24965–76. https://doi.org/10.1016/j.ijhydene.2021.05.065.
[12] Almomani F, Shawaqfah M, Alkasrawi M. Solar-driven hydrogen production from a water-splitting cycle based on carbon-TiO_2 nano-tubes. Int J Hydrogen Energy 2022;47:3294–305.
[13] Lan Q, Jin S, Yang B, Zhao Q, Si C, Xie H, et al. Metal-oxo cluster catalysts for photocatalytic water splitting and carbon dioxide reduction. Trans Tianjin Univ 2022;28:214–25. https://doi.org/10.1007/s12209-022-00324-z.
[14] Nemiwal M, Gosu V, Zhang TC, Kumar D. Metal organic frameworks as electrocatalysts: hydrogen evolution reactions and overall water splitting. Int J Hydrogen Energy 2021;46:10216–38. https://doi.org/10.1016/j.ijhydene.2020.12.146.
[15] Saji VS. A mini-review on transition metals-based 1D nanotubular bifunctional electrocatalysts for overall water splitting. Int J Hydrogen Energy 2022;47:32372–93. https://doi.org/10.1016/j.ijhydene.2022.07.163.
[16] Shandilya P, Sharma R, Arya RK, Kumar A, Vo D-VN, Sharma G. Recent progress and challenges in photocatalytic water splitting using layered double hydroxides (LDH) based nanocomposites. Int J Hydrogen Energy 2022;47:37438–75. https://doi.org/10.1016/j.ijhydene.2021.08.190.
[17] Reddy CV, Reddy KR, Shetti NP, Shim J, Aminabhavi TM, Dionysiou DD. Hetero-nanostructured metal oxide-based hybrid photocatalysts for enhanced photoelectrochemical water splitting – a review. Int J Hydrogen Energy 2020;45:18331–47. https://doi.org/10.1016/j.ijhydene.2019.02.109.
[18] Fajrina N, Tahir M. A critical review in strategies to improve photocatalytic water splitting towards hydrogen production. Int J Hydrogen Energy 2019;44:540–77. https://doi.org/10.1016/j.ijhydene.2018.10.200.
[19] Lin K, Wang X, Zhang Q, Fang C, Zhou J. An emerging bidirectional auxetic post-phosphorene ε-SnO monolayer: a promising Janus semiconductor with photocatalytic activity for solar-driven water splitting reaction. Int J Hydrogen Energy 2022;47:24761–76. https://doi.org/10.1016/j.ijhydene.2022.05.236.
[20] Yao S, Zhang X, Zhang Z, Chen A, Zhou Z. 2D Triphosphides: SbP_3 and GaP_3 monolayer as promising photocatalysts for water splitting. Int J Hydrogen Energy 2019;44:5948–54. https://doi.org/10.1016/j.ijhydene.2019.01.106.
[21] Zhang X, Zhang Z, Wu D, Zhang X, Zhao X, Zhou Z. Computational screening of 2D materials and rational design of heterojunctions for water splitting photocatalysts. Small Methods 2018;2:1700359. https://doi.org/10.1002/smtd.201700359.
[22] Nemiwal M, Zhang TC, Kumar D. Graphene-based electrocatalysts: hydrogen evolution reactions and overall water splitting. Int J Hydrogen Energy 2021;46:21401–18. https://doi.org/10.1016/j.ijhydene.2021.04.008.

Please cite this article as: Sukhanova EV et al., Novel Janus 2D structures of XMoY (X, Y = O, S, Se, Te) composition for solar hydrogen production, International Journal of Hydrogen Energy, https://doi.org/10.1016/j.ijhydene.2022.12.286

[23] Bozheyev F. Transition metal dichalcogenide thin films for solar hydrogen production. Current Opinion in Electrochemistry 2022:100995. https://doi.org/10.1016/j.coelec.2022.100995.
[24] Fathipour S, Ma N, Hwang WS, Protasenko V, Vishwanath S, Xing HG, et al. Exfoliated multilayer $MoTe_2$ field-effect transistors. Appl Phys Lett 2014;105:192101. https://doi.org/10.1063/1.4901527.
[25] Ni M, Leung MK, Leung DY, Sumathy K. A review and recent developments in photocatalytic water-splitting using TiO_2 for hydrogen production. Renew Sustain Energy Rev 2007;11:401–25. https://doi.org/10.1016/j.rser.2005.01.009.
[26] Peng R, Ma Y, Huang B, Dai Y. Two-dimensional Janus PtSSe for photocatalytic water splitting under the visible or infrared light. J Mater Chem 2019;7:603–10. https://doi.org/10.1039/C8TA09177C.
[27] Ju L, Bie M, Shang J, Tang X, Kou L. Janus transition metal dichalcogenides: a superior platform for photocatalytic water splitting. J Phys: Materials 2020;3:022004. https://doi.org/10.1088/2515-7639/ab7c57.
[28] Tang X, Kou L. 2D janus transition metal dichalcogenides: properties and applications. Phys Status Solidi 2022;259:2100562. https://doi.org/10.1002/pssb.202100562.
[29] Lu A-Y, Zhu H, Xiao J, Chuu C-P, Han Y, Chiu M-H, et al. Janus monolayers of transition metal dichalcogenides. Nat Nanotechnol 2017;12:744–9. https://doi.org/10.1038/nnano.2017.100.
[30] Li X, Li Z, Yang J. Proposed photosynthesis method for producing hydrogen from dissociated water molecules using incident near-infrared light. Phys Rev Lett 2014;112:018301. https://doi.org/10.1103/PhysRevLett.112.018301.
[31] Dong L, Lou J, Shenoy VB. Large in-plane and vertical piezoelectricity in janus transition metal dichalchogenides. ACS Nano 2017;11:8242–8. https://doi.org/10.1021/acsnano.7b03313.
[32] Zhang Y, Sa B, Miao N, Zhou J, Sun Z. Computational mining of Janus Sc_2C-based MXenes for spintronic, photocatalytic, and solar cell applications. J Mater Chem 2021;9:10882–92. https://doi.org/10.1039/D1TA00614B.
[33] Zhong Q, Dai Z, Liu J, Zhao Y, Meng S. Phonon thermal transport in Janus single layer M_2XY (M = Ga; X, Y = S, Se, Te): a study based on first-principles. Phys E Low-dimens Syst Nanostruct 2020;115:113683. https://doi.org/10.1016/j.physe.2019.113683.
[34] Yin W, Tan H, Ding P, Wen B, Li X-B, Teobaldi G, et al. Recent advances in low-dimensional janus materials: a theory and simulation perspective. Materials Advances 2021. https://doi.org/10.1039/D1MA00660F.
[35] Li R, Cheng Y, Huang W. Recent progress of Janus 2D transition metal chalcogenides: from theory to experiments. Small 2018;14:1802091. https://doi.org/10.1002/smll.201802091.
[36] Tang X, Li S, Ma Y, Du A, Liao T, Gu Y, et al. Distorted Janus transition metal dichalcogenides: stable two-dimensional materials with sizable band gap and ultrahigh carrier mobility. J Phys Chem C 2018;122:19153–60. https://doi.org/10.1021/acs.jpcc.8b04161.
[37] Zhang L, Xia Y, Li X, Li L, Fu X, Cheng J, et al. Janus two-dimensional transition metal dichalcogenides. J Appl Phys 2022;131:230902. https://doi.org/10.1063/5.0095203.
[38] Lu A-Y, Zhu H, Xiao J, Chuu C-P, Han Y, Chiu M-H, et al. Janus monolayers of transition metal dichalcogenides. Nat Nanotechnol 2017;12:744–9.
[39] Zhang J, Jia S, Kholmanov I, Dong L, Er D, Chen W, et al. Janus monolayer transition-metal dichalcogenides. ACS Nano 2017;11:8192–8.
[40] Zhang Y, Ye H, Yu Z, Liu Y, Li Y. First-principles study of square phase MX_2 and Janus MXY (M=Mo, W; X, Y=S, Se, Te) transition metal dichalcogenide monolayers under biaxial strain. Phys E Low-dimens Syst Nanostruct 2019;110:134–9. https://doi.org/10.1016/j.physe.2019.02.009.
[41] Yagmurcukardes M, Sevik C, Peeters FM. Electronic, vibrational, elastic, and piezoelectric properties of monolayer Janus MoSTe phases: a first-principles study. Phys Rev B 2019;100:045415. https://doi.org/10.1103/PhysRevB.100.045415.
[42] Wang Z. 2H→1T′ phase transformation in Janus monolayer MoSSe and MoSTe: an efficient hole injection contact for 2H-MoS_2. J Mater Chem C 2018;6:13000–5.
[43] Ahmad I, Shahid I, Ali A, Ruan Z, Yan C, Ali J, et al. Two dimensional Janus SGaInSe(SeGaInS)/$PtSe_2$ van der Waals heterostructures for optoelectronic and photocatalytic water splitting applications. Int J Hydrogen Energy 2022;47:28833–44. https://doi.org/10.1016/j.ijhydene.2022.06.188.
[44] Wang G, Chen C, Teketel BS, Xu B, Lin B. Constructing a new 2D Janus black phosphorus/SMoSe heterostructure for spontaneous wide-spectral-responsive photocatalytic overall water splitting. Int J Hydrogen Energy 2021;46:39183–94.
[45] Bao J, Zhu B, Zhang F, Chen X, Guo H, Qiu J, et al. Sc_2CF_2/Janus MoSSe heterostructure: a potential Z-scheme photocatalyst with ultra-high solar-to-hydrogen efficiency. Int J Hydrogen Energy 2021;46:39830–43.
[46] Gavryushkin P, Sagatov N, Sukhanova E, Medrish I, Popov Z. Janus structures of SMoSe and SVSe compositions with low enthalpy and unusual crystal chemistry. J Appl Crystallogr 2022;55:1324–35. https://doi.org/10.1107/S1600576722008202.
[47] Hohenberg P, Kohn W. Inhomogeneous electron gas. Phys Rev 1964;136:B864–71. https://doi.org/10.1103/PhysRev.136.B864.
[48] Kohn W, Sham LJ. Self-consistent equations including exchange and correlation effects. Phys Rev 1965;140:A1133–8. https://doi.org/10.1103/PhysRev.140.A1133.
[49] Kresse G, Furthmüller J. Efficient iterative schemes for ab initio total-energy calculations using a plane-wave basis set. Phys Rev B 1996;54:11169–86.
[50] Kresse G, Furthmüller J. Efficiency of ab-initio total energy calculations for metals and semiconductors using a plane-wave basis set. Comput Mater Sci 1996;6:15–50. https://doi.org/10.1016/0927-0256(96)00008-0.
[51] Kresse G, Hafner J. Ab initio molecular-dynamics simulation of the liquid-metal-amorphous-semiconductor transition in germanium. Phys Rev B 1994;49:14251–69. https://doi.org/10.1103/PhysRevB.49.14251.
[52] Perdew JP, Burke K, Ernzerhof M. Generalized gradient approximation made simple. Phys Rev Lett 1996;77:3865–8. https://doi.org/10.1103/PhysRevLett.77.3865.
[53] Blöchl PE. Projector augmented-wave method. Phys Rev B 1994;50:17953–79. https://doi.org/10.1007/BF02712785.
[54] Monkhorst HJ, Pack JD. Special points for Brillouin-zone integrations. Phys Rev B 1976;13:5188–92. https://doi.org/10.1103/PhysRevB.13.5188.
[55] Krukau AV, Vydrov OA, Izmaylov AF, Scuseria GE. Influence of the exchange screening parameter on the performance of screened hybrid functionals. J Chem Phys 2006;125:224106. https://doi.org/10.1063/1.2404663.
[56] Momma K, Izumi F. VESTA 3 for three-dimensional visualization of crystal, volumetric and morphology data. J Appl Crystallogr 2011;44:1272–6. https://doi.org/10.1107/S0021889811038970.
[57] Togo A, Tanaka I. First principles phonon calculations in materials science. Scripta Mater 2015;108:1–5. https://doi.org/10.1016/j.scriptamat.2015.07.021.

Please cite this article as: Sukhanova EV et al., Novel Janus 2D structures of XMoY (X, Y = O, S, Se, Te) composition for solar hydrogen production, International Journal of Hydrogen Energy, https://doi.org/10.1016/j.ijhydene.2022.12.286

[58] Bader RF. Atoms in molecules. Acc Chem Res 1985;18:9–15. https://doi.org/10.1021/ar00109a003.
[59] Henkelman GA, Arnaldsson A, Jónsson H. A fast and robust algorithm for Bader decomposition of charge density. Comput Mater Sci 2006;36:354–60. https://doi.org/10.1016/j.commatsci.2005.04.010.
[60] Olsen R, Kroes G, Henkelman G, Arnaldsson A, Jónsson H. Comparison of methods for finding saddle points without knowledge of the final states. J Chem Phys 2004;121:9776–92. https://doi.org/10.1063/1.1809574.
[61] Henkelman G, Jónsson H. Improved tangent estimate in the nudged elastic band method for finding minimum energy paths and saddle points. J Chem Phys 2000;113:9978–85. https://doi.org/10.1063/1.1323224.
[62] Clark SJ, Segall MD, Pickard CJ, Hasnip PJ, Probert MI, Refson K, et al. First principles methods using CASTEP. Z für Kristallogr - Cryst Mater 2005;220:567–70. https://doi.org/10.1524/zkri.220.5.567.65075.
[63] Refson K, Tulip PR, Clark SJ. Variational density-functional perturbation theory for dielectrics and lattice dynamics. Phys Rev B 2006;73:155114. https://doi.org/10.1103/PhysRevB.73.155114.
[64] Oreshonkov AS, Sukhanova EV, Popov ZI. Raman spectroscopy of janus MoSSe monolayer polymorph modifications using density functional theory. Materials 2022;15:3988. https://doi.org/10.3390/ma15113988.
[65] Sun Y, Shuai Z, Wang D. Janus monolayer of WSeTe, a new structural phase transition material driven by electrostatic gating. Nanoscale 2018;10:21629–33. https://doi.org/10.1039/C8NR08151D.
[66] Haga T, Fujimoto Y, Saito S. Electronic structure and scanning tunneling microscopy images of heterostructures consisting of graphene and carbon-doped hexagonal boron nitride layers. Phys Rev B 2019;100:125403. https://doi.org/10.1103/PhysRevB.100.125403.
[67] Vanpoucke DEP, Brocks G. Formation of Pt-induced Ge atomic nanowires on Pt/Ge(001): a density functional theory study. Phys Rev B 2008;77:241308. https://doi.org/10.1103/PhysRevB.77.241308.
[68] Eriksson F, Fransson E, Erhart P. The hiphive package for the extraction of high-order force constants by machine learning. Advanced Theory and Simulations 2019;2:1800184. https://doi.org/10.1002/adts.201800184.
[69] Born M. On the stability of crystal lattices. In: I. Mathematical proceedings of the Cambridge philosophical society, 36. Cambridge University Press; 1940. p. 160–72.
[70] Born M, Misra RD. On the stability of crystal lattices. In: IV. Mathematical proceedings of the Cambridge philosophical society, 36. Cambridge University Press; 1940. p. 466–78. https://doi.org/10.1017/S0305004100017138.
[71] Andrew RC, Mapasha RE, Ukpong AM, Chetty N. Mechanical properties of graphene and boronitrene. Phys Rev B 2012;85:125428. https://doi.org/10.1103/PhysRevB.85.125428.
[72] Yagmurcukardes M, Peeters FM. Stable single layer of Janus MoSO: strong out-of-plane piezoelectricity. Phys Rev B 2020;101:155205. https://doi.org/10.1103/PhysRevB.101.155205.
[73] Pham TH, Ullah H, Shafique A, Kim HJ, Shin Y-H. Enhanced out-of-plane electromechanical response of Janus ZrSeO. Phys Chem Chem Phys 2021;23:16289–95. https://doi.org/10.1039/D1CP00119A.
[74] Xia J, Wang J, Chao D, Chen Z, Liu Z, Kuo J-L, et al. Phase evolution of lithium intercalation dynamics in 2H-MoS_2. Nanoscale 2017;9:7533–40. https://doi.org/10.1039/C7NR02028G.
[75] Nasr Esfahani D, Leenaerts O, Sahin H, Partoens B, Peeters FM. Structural transitions in monolayer MoS_2 by lithium adsorption. J Phys Chem C 2015;119:10602–9. https://doi.org/10.1021/jp510083w.
[76] Guo Y, Sun D, Ouyang B, Raja A, Song J, Heinz TF, et al. Probing the dynamics of the metallic-to-semiconducting structural phase transformation in MoS_2 crystals. Nano Lett 2015;15:5081–8. https://doi.org/10.1021/acs.nanolett.5b01196.
[77] Lin Y-C, Dumcenco DO, Huang Y-S, Suenaga K. Atomic mechanism of the semiconducting-to-metallic phase transition in single-layered MoS_2. Nat Nanotechnol 2014;9:391–6. https://doi.org/10.1038/nnano.2014.64.
[78] Zhang S, Zhang N, Zhao Y, Cheng T, Li X, Feng R, et al. Spotting the differences in two-dimensional materials – the Raman scattering perspective. Chem Soc Rev 2018;47:3217–40. https://doi.org/10.1039/C7CS00874K.
[79] Gajdoš M, Hummer K, Kresse G, Furthmüller J, Bechstedt F. Linear optical properties in the projector-augmented wave methodology. Phys Rev B 2006;73:045112. https://doi.org/10.1103/PhysRevB.73.045112.
[80] Eberlein T, Bangert U, Nair RR, Jones R, Gass M, Bleloch AL, et al. Plasmon spectroscopy of free-standing graphene films. Phys Rev B 2008;77:233406. https://doi.org/10.1103/PhysRevB.77.233406.
[81] Cui Z, Bai K, Ding Y, Wang X, Li E, Zheng J, et al. Electronic and optical properties of janus MoSSe and ZnO vdWs heterostructures. Superlattice Microst 2020;140:106445. https://doi.org/10.1016/j.spmi.2020.106445.
[82] Lou J, Ren K, Huang Z, Huo W, Zhu Z, Yu J. Electronic and optical properties of two-dimensional heterostructures based on Janus XSSe (X = Mo, W) and $Mg(OH)_2$: a first principles investigation. RSC Adv 2021;11:29576–84. https://doi.org/10.1039/D1RA05521F.
[83] Barakat F, Laref A, AlSalhi MS, Faraji S. The impact of anion elements on the engineering of the electronic and optical characteristics of the two dimensional monolayer janus MoSSe for nanoelectronic device applications. Results Phys 2020;18:103284. https://doi.org/10.1016/j.rinp.2020.103284.
[84] Habibi M, Zabihi F, Ahmadian-Yazdi MR, Eslamian M. Progress in emerging solution-processed thin film solar cells—Part II: perovskite solar cells. Renew Sustain Energy Rev 2016;62:1012–31. https://doi.org/10.1016/j.rser.2016.05.042.
[85] Chen E M, Williams L, Olvera A, Zhang C, Zhang M, Shi G, et al. Sustainable p-type copper selenide solar material with ultra-large absorption coefficient. Chem Sci 2018;9:5405–14. https://doi.org/10.1039/C8SC00873F.
[86] Ju L, Dai Y, Wei W, Li M, Huang B. DFT investigation on two-dimensional GeS/WS_2 van der Waals heterostructure for direct Z-scheme photocatalytic overall water splitting. Appl Surf Sci 2018;434:365–74. https://doi.org/10.1016/j.apsusc.2017.10.172.
[87] Fu C-F, Luo Q, Li X, Yang J. Two-dimensional van der Waals nanocomposites as Z-scheme type photocatalysts for hydrogen production from overall water splitting. J Mater Chem 2016;4:18892. https://doi.org/10.1039/C6TA08769H. –8.
[88] Chakrapani V, Angus JC, Anderson AB, Wolter SD, Stoner BR, Sumanasekera GU. Charge transfer equilibria between diamond and an aqueous oxygen electrochemical redox couple. Science 2007;318:1424–30. https://doi.org/10.1021/acs.nanolett.8b02561.
[89] Fu C-F, Sun J, Luo Q, Li X, Hu W, Yang J. Intrinsic electric fields in two-dimensional materials boost the solar-to-hydrogen efficiency for photocatalytic water splitting. Nano Lett 2018;18:6312–7.
[90] Yang W, Park J, Kwon H-C, Hutter OS, Phillips LJ, Tan J, et al. Solar water splitting exceeding 10% efficiency via low-cost Sb_2Se_3 photocathodes coupled with semitransparent perovskite photovoltaics. Energy Environ Sci 2020;13:4362–70. https://doi.org/10.1039/D0EE02959A.

Please cite this article as: Sukhanova EV et al., Novel Janus 2D structures of XMoY (X, Y = O, S, Se, Te) composition for solar hydrogen production, International Journal of Hydrogen Energy, https://doi.org/10.1016/j.ijhydene.2022.12.286

[91] Ju L, Bie M, Tang X, Shang J, Kou L. Janus WSSe monolayer: an excellent photocatalyst for overall water splitting. ACS Appl Mater Interfaces 2020;12:29335–43. https://doi.org/10.1038/nnano.2014.64.
[92] Jakhar M, Kumar A, Ahluwalia PK, Tankeshwar K, Pandey R. Engineering 2D materials for photocatalytic water-splitting from a theoretical perspective. Materials 2022;15:2221. https://doi.org/10.3390/ma15062221.
[93] Jia J, Seitz LC, Benck JD, Huo Y, Chen Y, Ng JWD, et al. Solar water splitting by photovoltaic-electrolysis with a solar-to-hydrogen efficiency over 30. Nat Commun 2016;7:1–6. https://doi.org/10.1038/ncomms13237.
[94] Deng S, Sumant AV, Berry V. Strain engineering in two-dimensional nanomaterials beyond graphene. Nano Today 2018;22:14–35. https://doi.org/10.1016/j.nantod.2018.07.001.
[95] Sukhanova EV, Sorokin PB. Specific response of the atomic and electronic structure of $Ta_2Pd_3Se_8$ and $Ta_2Pt_3Se_8$ nanoribbons to the uniaxial strain. J Phys Chem C 2020;124:7539–43. https://doi.org/10.1021/acs.jpcc.0c00245.
[96] Gan X, Lei D, Wong K-Y. Two-dimensional layered nanomaterials for visible-light-driven photocatalytic water splitting. Mater Today Energy 2018;10:352–67. https://doi.org/10.1016/j.mtener.2018.10.015Strain Engineering: A Boosting Strategy for Photocatalysis.
[97] Miao Y, Zhao Y, Zhang S, Shi R, Zhang T. Strain engineering: a boosting strategy for photocatalysis. Adv Mater 2022:2200868. https://doi.org/10.1002/adma.202200868.

Please cite this article as: Sukhanova EV et al., Novel Janus 2D structures of XMoY (X, Y = O, S, Se, Te) composition for solar hydrogen production, International Journal of Hydrogen Energy, https://doi.org/10.1016/j.ijhydene.2022.12.286